Heavy Ion Nuclear Reaction Impact on SEE Testing: From Standard to Ultra-high Energies

Vanessa Wyrwoll, Rubén García Alía, Ketil Røed, Pablo Fernández-Martínez, Maria Kastriotou, Matteo Cecchetto, Nourdine Kerboub, Maris Tali, and Francesco Cerutti

***Abstract*— We perform Monte Carlo (MC) simulations to describe heavy ion (HI) nuclear interactions in a broad energy range (4 MeV/n–150 GeV/n), focusing on the single event effect (SEE) sub-linear energy transfer (LET) impact. Previously retrieved single event latch-up (SEL) experimental data have indicated that standard energy ions (∼10 MeV/n) can produce high-LET secondaries through fusion reactions which are expected to strongly influence the SEE cross section in the sub-LET region. Alternatively, interactions of higher energy ions (>100 MeV/n) yield secondaries of a similar LET distribution as from the projectile, for projectile-like fragments, and high-energy proton reactions, for target-like fragments. Hence, the factor of relevance to the sub-LET SEE cross section is correlated to low-energy.**

***Index Terms*— CERN, FLUKA, Monte Carlo (MC) simulation, single event effects (SEEs).**

I. Introduction

INDIRECT energy deposition plays an important role in single event effect (SEE) rate calculations, as indicated by Dodd *et al.* [1]. Looking into the galactic cosmic ray (GCR) high energy environment, it has been pointed out in [2] and [3], through Monte Carlo (MC) simulations and in-flight data, that an underestimation of up to two orders of magnitude of the in-flight SEE rate could occur if the indirect energy deposition events caused by nuclear interactions are not taken into account. These interactions are considered to be originated from ions with insufficient linear energy transfer (LET) to induce SEE through direct ionization, thus referred to as sub-LET threshold ions in the following. This underestimation derives from the use of standard SEE prediction models which exclude the heavy ion (HI) nuclear reaction contribution. In the mentioned studies [2], [3], the component is modeled with a large amount of tungsten (high-Z material) close to the sensitive volume (SV) and a large LET threshold value. As will be discussed in this work, parameters such as the composition of material close to the SV and the actual SV size are relevant when it comes to SEE rate and beam fragmentation. Furthermore, these assumptions have been previously discussed by Peterson [4] using a simple double-Weibull approach. By comparing in-flight data with the standard approach, which only indirectly considers the contribution of nuclear interactions originated from HIs, the contribution of sub-LET threshold effects (nuclear interactions) to the GCR SEE rate is limited to approximately 15% in total. There, the difference between the model and the measured data can be explained by the application of a rectangular parallel-piped (RPP) model, instead of the more appropriate integral-RPP (IRPP), which is used in [3]. Since the IRPP includes variation of critical charge values, it represents an extension of the RPP. However, similar to the RPP model, the IRPP model is also constructed to model direct ionization and not nuclear interaction mechanisms in the sub-LET threshold region.

In [4], using the IRPP model, the energy deposition distribution simulated using a RPP geometry is convolved with the experimental HI SEE cross section curve. A successful prediction of the proton single event upset (SEU) and single event latch-up (SEL) cross section has been carried out in [3], by utilizing an IRPP-MC model, based on the HI direct ionization response. Unfortunately, this approach has not been fruitful in achieving a similar accuracy for sub-LET threshold low-energy HI data as it was for high-energy ions or protons.

Therefore, this work investigates the differences among high energy proton and HI beams, the latter from standard energies to ultrahigh energy (UHE) in terms of nuclear fragmentation and their impact on the SEE cross section. Simulations and models to estimate the effects of the GCR environment on the SEE rate, are gaining more attention and relevance, as pointed out in previous work, such as by Pellish *et al.* [5]. Hence, this article is focused on MC FLUKA [6] simulations and comparing them to measurements carried out in test facilities representative of the GCR environment.

In this sense, the UHE HI beams provided by CERN in 2017 (xenon) and 2018 (lead) have offered the unique possibility for carrying out the mentioned tests. Two different test areas, the CERN high energy accelerator mixed-field (CHARM) [7] facility and the Super Proton Synchrotron North Experimental Area (SPS-NA) [8] were used. Specifically, UHE xenon and lead ion beams of 6.3 and 5.4 GeV/n, respectively, were delivered at CHARM; whereas even higher energies between 19 and 75 GeV/n for xenon and 150 GeV/n for lead were used in the SPS-NA. As will be pointed out later, these very unique beams lead to a production of projectile-like and fission

Manuscript received December 20, 2019; revised January 27, 2020, February 3, 2020, and February 6, 2020; accepted February 8, 2020. Date of publication February 12, 2020; date of current version July 16, 2020. This work was supported by RADSAGA through the European Union's Horizon 2020 Research and Innovation Program under Grant 721624.

Vanessa Wyrwoll, Rubén García Alía, Pablo Fernández-Martínez, Maria Kastriotou, Matteo Cecchetto, Nourdine Kerboub, Maris Tali, and Francesco Cerutti are with CERN, 1211 Geneva, Switzerland (e-mail: vanessa.wyrwoll@cern.ch).

Ketil Røed is with the Department of Physics, University of Oslo, 0315 Oslo, Norway.

Color versions of one or more of the figures in this article are available online at http://ieeexplore.ieee.org.

Digital Object Identifier 10.1109/TNS.2020.2973591

fragments, when interacting with material in the beam line. These interaction products have energies per nucleon around those of the primary beam, and therefore relatively low LET values. Hence, high LET particles of relevance for the sub-LET region are low-energy target-like fragments, independent of the projectile Z.

The high energy range, which is considered between 10 and 100 MeV per nucleon, is offered by facilities like Texas A&M University (TAMU) [9], Berkeley Accelerator Space Effects (BASE) [10], Grand Accélérateur National d'Ions Lourds (GANIL) [11], and Kernfysisch Versneller Instituut (KVI) [12]. Beams that reach even higher energies between 100 MeV/n and 5 GeV/n, referred to as very high energies, can be provided by Gesellschaft für Schwerionenforschung (GSI) [13] or NASA Space Radiation Laboratory (NSRL) [14].

Since protons have been postulated to be a dominating factor with regard to the sub-LET contribution in the GCR environment [3], high energy protons are especially addressed in this work. In particular, MC simulations and experimental data with 200-MeV protons gathered at the Paul Scherrer Institut (PSI) [15] in Switzerland, are compared.

Moreover, standard energy HI tests ($\sim$10 MeV/n) are important for space application since the LET is comparable to ions present in the GCR environment. Therefore, this article includes a comparison between the theoretical contribution of standard energies of neon and argon beams, obtained through MC FLUKA simulations, and the experimental data obtained for the same species at the RADiation Effects Facility (RADEF) in Finland [16] and the Université Catholique de Leuven (UCL), in Belgium [17]. It will be further discussed in this work, that standard energy HIs, while interacting with material in the beam line, are leading to high-LET fragments originated from fusion processes. These fragments dominate the SEE cross sections within the sub-LET region.

II. HI Nuclear Reaction Products

Typical SEE tests are carried out in dedicated standard energy HI and high-energy proton beams. In the context of this article, standard energies are considered as up to 10 MeV/n. Especially in the case of ions, this energy range is below the energies predominant in the space environment, where the energy regime goes up to several GeV/n. The standard approach to derive the in-orbit SEE rate from the experimental cross section as a function of LET, convolved with the LET spectrum is done by extrapolating all possible LET values found in realistic applications. This approach does not consider the associated Z and primary energy of the ions. These parameters can vary significantly from test to test and when compared to real radiation environments. Nevertheless, they can play an important role with regard to SEE production, especially through nuclear reactions. Therefore, the applicability of this approach is discussed in the following *via* experimental data and MC simulations. Although this article focusses on simulation tools, it is important to underline the experimentally indicated implications, such as the experienced effects discussed by Koga *et al.* [18], where beam fragmentation was observed during LET distribution measurements of Bevalac ion beams.

TABLE I
Simulation Parameters Applied in This Article

Particle	Particle Properties		
	Energy	*Projected Range in Si [μm]*	*Projected Range in W [μm]*
^{20}Ne	9.3 MeV/n	1.512×10^{2}	4.050×10^{1}
^{40}Ar	9.3 MeV/n	1.185×10^{2}	3.237×10^{1}
^{130}Xe	40 GeV/n	4.942×10^{6}	9.555×10^{5}
^{208}Pb	150 GeV/n	1.359×10^{7}	2.577×10^{6}
Protons	200 MeV	1.354×10^{5}	3.901×10^{4}

A. Simulations

In this article, the nuclear reaction fragments through Z, LET, and kinetic energy distribution are simulated for chosen energies and particles using the FLUKA MC code [6], [19], [20].

FLUKA is well-benchmarked and widely used to reliably simulate the particle interaction with matter, covering a broad energy range and particle repertoire [6]. In order to simulate the particle interactions in different energy ranges and particle species, various physical models need to be implemented and embedded within the FLUKA code. By performing the simulations, the user needs to choose the required options, by setting up the input for the calculations. In general, the following codes are implemented for this purpose according to the particle energy.

1) For energies above 5-GeV/n hadronic collisions need to be treated differently than for lower energies. There, soft multiparticle production, meaning particles with low traverse momenta are involved. For this purpose, the MC event generator Dual Parton Model and Jets (DPMJETs III) [21] has to be applied to the simulation to ensure a proper simulation of nucleus-nucleus events.
2) Energies below 5 GeV/n and above 125 MeV/n are mimicked through a relativistic quantum molecular dynamic (RQMD) code. This code is implemented in FLUKA via a modified version of RQMD-2.4 [22].
3) The nuclear interactions in the ion energy range up to 125 MeV/n are modeled using the Boltzmann master equation (BME) [23].

In this article, the public FLUKA version FLUKA2011 version 2x.6 Mar-19 was used. Furthermore, electromagnetic dissociation was activated for both the projectile and target ions.

Not only the input parameters need to be chosen according to the simulation, but also the geometry and material play a relevant role to estimate theoretically possible results. For instance, in modern microcircuits very small thicknesses of silicon, around several tens of nanometers, are common. However, in order to investigate and focus on beam fragmentation mechanisms and general physical phenomena in silicon, a target thickness large enough to absorb the deposited energy by the fragments of interest, is relevant. Table I illustrates the simulated particles, their kinetic energy, and the projected

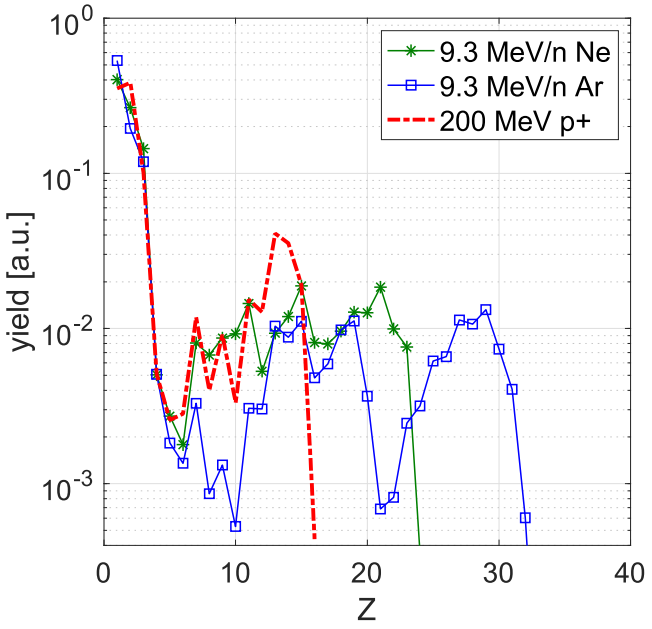

Fig. 1. Full Z distribution of standard energy HI (^{20}Ne and ^{40}Ar) fragmentation in comparison to high energy protons on a 140-μm silicon target, as obtained from FLUKA MC simulations.

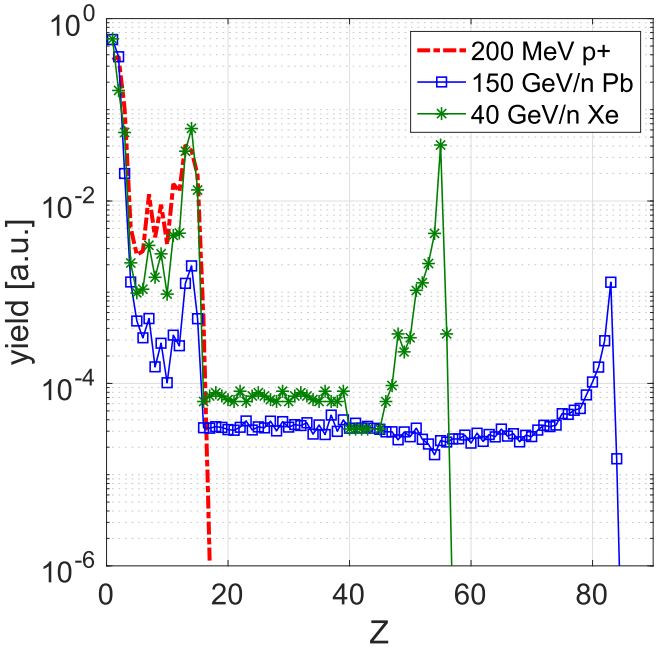

Fig. 2. Full Z distribution of UHE HI (^{130}Xe and ^{208}Pb) fragmentation in comparison to high energy protons on a 140-μm silicon target, as obtained from FLUKA MC simulations.

range in silicon and tungsten [24]. In this article, a 140-μm silicon target has been chosen to represent the scoring volume in our simulations. The selection of the thickness is based on the charge collection depth of a silicon diode used in the study, but not presented in this article [25]. It is also considered as a good compromise for being thick enough for retrieving a significant amount of nuclear reactions, but not too thick that inelastic reactions are no longer dominated by the primary beam. For example, provided the inelastic interaction length of UHE lead ions in silicon is 6 cm, in a thickness of 140 μm, only 0.23% of them are expected to interact.

B. Z Distributions for High Energy Proton, Standard, and UHE HI Beams

This article is focused on the 200-MeV protons of PSI [13], the 9.3-MeV/n ^{20}Ne, and ^{40}Ar ions of RADEF [14], as well as the 40-GeV/n ^{130}Xe and 150-GeV/n ^{208}Pb UHE ion beams delivered at CERN [7], [8], [26] as mentioned previously in this article. Neon and argon ions have been chosen because with a LET value of 3.7 and 10.1 MeVcm^2/mg, respectively, they are comparable to the UHE xenon (3.6 MeVcm^2/mg) and lead (8.8 MeVcm^2/mg) ions used in this article. Figs. 1 and 2 show the full Z distribution of nuclear products of these ions when interacting with silicon. Specifically, Fig. 1 displays the low-energy 9.3-MeV/n neon and argon nuclear products in silicon, in comparison to the products obtained with high-energy protons, as simulated in FLUKA. Correspondingly in Fig. 2, the UHE xenon and lead ion products are compared to the proton production.

In Fig. 1, the distribution in Z of the argon fragments shows two discernible peaks, around Z values of 14 and 30, respectively. The target is made of silicon with an atomic number of 14. Therefore, the first peak can be attributed to target-like fragments, whereas the second one shows an atomic number even higher than both the primary ($Z_{\mathrm{Ar}} = 18$) and target ($Z_{\mathrm{Si}} = 14$) particles, leading to the conclusion that it is due to fusion products, who's production is common in this energy regime [3]. In the same figure, neon has an atomic number of 10, close to silicon. Therefore, the nuclear production of target-like fragments overlaps the projectile fragment production. Fusion fragmentation occurs here as well, as represented by the plateau observed up to $Z = 20$. Again, the products in this region show higher Z than both the individual projectile and the target Z itself.

In the case of xenon (see Fig. 2), target-like and projectile-like fragmentation peaks can be identified, as well, around $Z = 14$ and 54, respectively. In turn, the nuclear fragment production of lead shows the two expected peaks around $Z = 14$ and 82, with a broader plateau in-between. It is worth noting that in the UHE regime fusion between the projectile and target ions does not take place. Though not shown in the plot, this is also the case for lighter ions, such as argon and neon, which however, as shown in Fig. 1, do undergo fusion at energies around 10 MeV/n.

Overall, it can be seen for both Figs. 1 and 2, that for Z between 1 and 20, the distributions for standard energy HIs (neon and argon) and UHE HIs (lead and xenon) are close to the high energy proton distribution, also represented in the corresponding figures.

In general, the Z distribution for ions, both UHE and standard energy, and protons are similar for silicon like material.

C. LET Distributions for High Energy Proton, Standard, and UHE HI Beams

The LET distribution of the fragments produced in silicon by the discussed beams was also studied in detail. Hence, the LET distribution for 9.3 MeV/n neon ions is illustrated

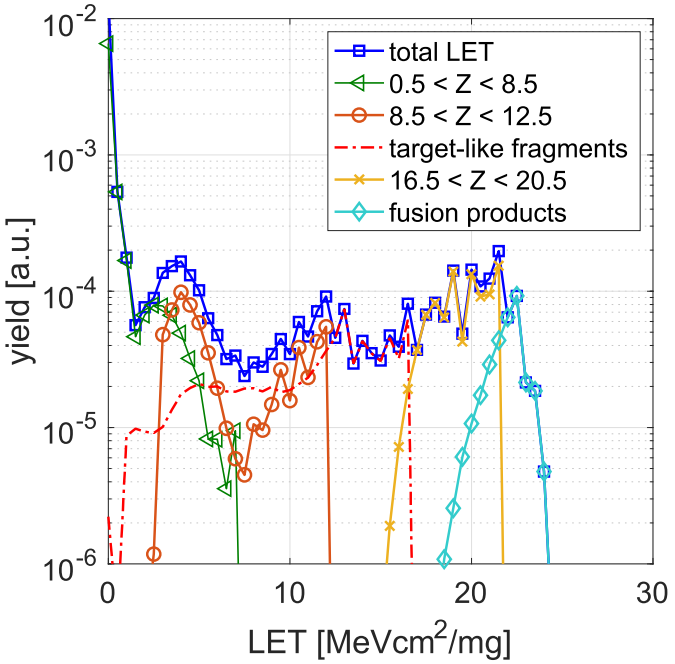

Fig. 3. LET distribution of 9.3-MeV/n ^{20}Ne fragmentation on a 140-μm silicon target, as obtained from FLUKA MC simulations.

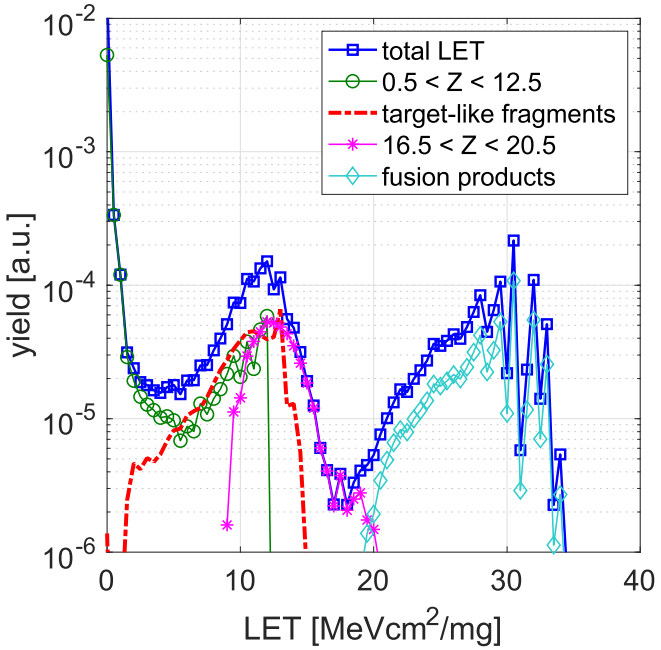

Fig. 4. LET distribution of 9.3-MeV/n ^{40}Ar fragmentation in a 140-μm silicon target, as obtained from FLUKA MC simulations.

in Fig. 3, disentangling the contribution of fragments with different Z ranges. In order to give a full overview of the occurring fragmentation, Z has been filtered and grouped according to 0.5–8.5, 8.5–12.5, 12.5–14.5 (target-like fragments), 16.5–20.5, and 20.5–30.5 (fusion products). Unlike the Z distribution, the LET distribution of the neon products does not show clearly distinguishable peaks. This can again be attributed to the fusion products ($20.5 < Z < 30.5$), which exhibit a LET peak value (22 MeVcm^2/mg) significantly above the possible LET of silicon fragments in silicon ($\sim$15 MeVcm^2/mg).

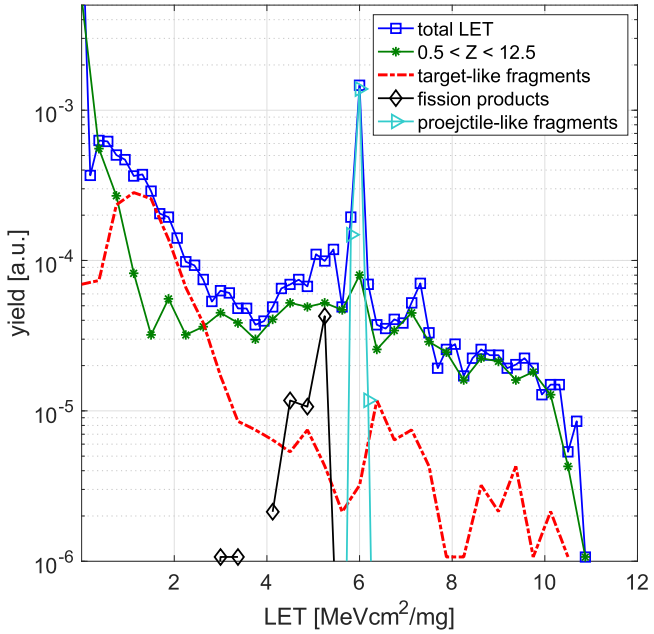

Fig. 5. LET distribution of 40-GeV/n ^{130}Xe fragmentation on a 140-μm silicon target, as obtained from FLUKA MC simulations.

As is the case, Figs. 3 and 4 show the LET distribution of 9.3-MeV/n argon. Again the fragmentation products are filtered in terms of their contribution: $0.5 < Z < 12.5$, $12.5 < Z < 14.5$ (target-like fragments), $16.5 < Z < 20.5$, and $20.5 < Z < 40.5$ (fusion products). On the contrary to neon in Fig. 3, the LET distribution of fragments for the 9.3-MeV/n argon case (Fig. 4) shows two peaks, where one comes from target-like fragments ($12.5 < Z < 16.5$) and the other one from fusion products ($20.5 < Z < 40.5$). These fusion products show a LET of up to 30 MeVcm^2/mg, which again is significantly higher than the possible LET of silicon fragments in silicon ($\sim$15 MeVcm^2/mg). Therefore, it can be concluded that the high LET fragments have a higher Z than the projectile or target in the case of neon and argon.

Looking at the UHE HI beams, Figs. 5 and 6 show the LET distribution of 40-GeV/n ^{130}Xe and 150-GeV/n ^{208}Pb fragments produced on a 140-μm silicon target, respectively, which correspond to the experimental conditions in the SPS-NA at CERN [7], [8]. The LET distributions show a separated peak at 6 and 15 MeVcm^2/mg for xenon and lead, respectively, which corresponds to the LET of the projectile particle. As opposed to the 9.3-MeV/n neon and argon cases (Figs. 3 and 4), the high LET fragments generated from the UHE xenon and lead ions are target-like in terms of Z, whereas the projectile like fragments ($52.5 < Z < 56.5$ for xenon and $80.5 < Z < 84.5$ for lead) show a low LET value, due to their very high kinetic energies, as will be further discussed later.

In Figs. 5 and 6, the LET distributions are selected again, as before for neon (Fig. 3) and argon (Fig. 4), according to their contribution to the specific total LET curve and in order to give a full impression of created fragments: from 0.5 to 12.5, from 12.5 to 16.5 (target-like fragments), fission products of 16.5 up to the beginning of the respective projectile-like fragments (52.5 for xenon and 80.5 for lead).

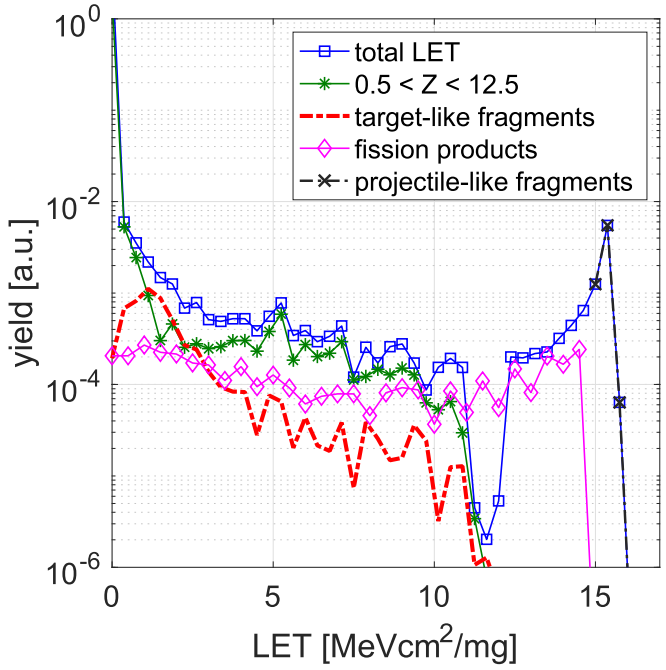

Fig. 6. LET distribution of 150-GeV/n ^{208}Pb fragmentation on a 140-μm silicon target, as obtained from FLUKA MC simulations.

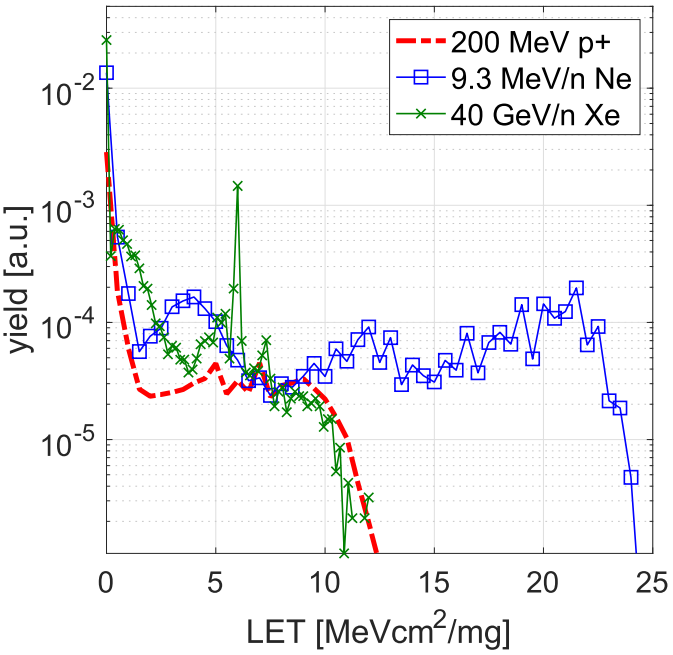

Fig. 7. LET distribution of HI and UHE beams (^{20}Ne and ^{130}Xe) fragmentation with comparable LET and 200-MeV protons, as obtained from FLUKA MC simulations.

In Fig. 7, the total LET distribution, including all Z fragmentation products, can be seen for 9.3-MeV/n ^{20}Ne and 40-GeV/n ^{130}Xe, which have similar LET in silicon. Here, the fragments can reach LET values above 25 MeVcm^2/mg due to fusion for standard energy ions, whereas the UHE HI LET distribution is more similar to that of high energy protons.

These observations are linked to the target-like fragment dominance in the high-LET region, which are thus the same (i.e., silicon-like) for high energy protons and UHE ions. Therefore, high energy ions produce a similar nuclear reaction product LET distribution as protons. The implications of such observation on the sub-LET threshold SEE results will be discussed in Sections III and IV.

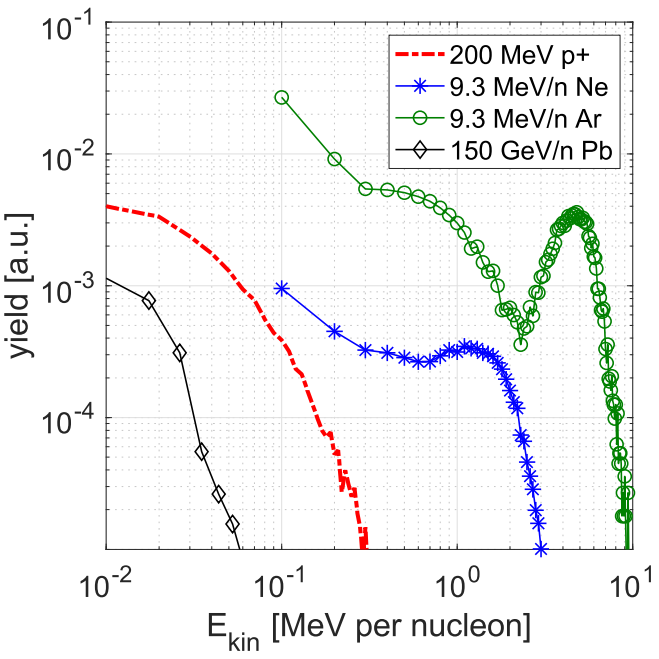

Fig. 8. Kinetic energy distribution of the fragments with $12.5 < Z < 16.5$ generated by 200-MeV protons, 9.3-MeV/n ^{20}Ne, 9.3-MeV/n ^{40}Ar, and 150-GeV/n ^{208}Pb ions, impinging on a 140-μm-thick silicon target.

D. Kinetic Energy Distributions for High Energy Proton, Standard, and UHE HI Beams

Additionally to the LET and Z distribution, the kinetic energy distribution of produced fragments is of main interest. Especially target-like fragments with Z between 13 and 16 are dominating the high-LET range for ion interactions in the UHE regime. Fig. 8 shows the kinetic energy distribution of nuclear reaction products with Z between 12.5 and 16.5, for the same proton and ion beams studied before. For argon, the created fragments can reach a kinetic energy per nucleon comparable to the primary particle (i.e., 9.3 MeV/n). In addition, neon fragments can reach a kinetic energy up to 3.6 MeV/n, but peaking at 2 MeV/n, which seems to be originated from target-like fragments, since their Z is near that of silicon.

Target-like fragments induced by 200-MeV protons have very low kinetic energy up to 400 keV/n, which corresponds to a LET value of 12.4 MeVcm^2/mg, close to the maximum LET of silicon in silicon (15 MeV/cm^2/mg), which is reached at 900 keV/n. UHE HIs, such as 40-GeV/n xenon and 150-GeV/n lead have been proven to generate target-like fragments with a very low kinetic energy of a few hundreds of keV/n, similar to 200-MeV protons: for ^{130}Xe a value of 200 keV/n and for ^{208}Pb 50 keV/n are reached, corresponding to LET values of 11.4 and 6.3 MeVcm^2/mg, respectively.

Focusing on the kinetic energy distribution of fusion fragments stemming from interactions between the ion and the material, the kinetic energy distribution goes up to 1.9 MeV/n for neon and 5.5 MeV/n for argon. Even if the kinetic energy of these products is lower than the projectile one, they show a

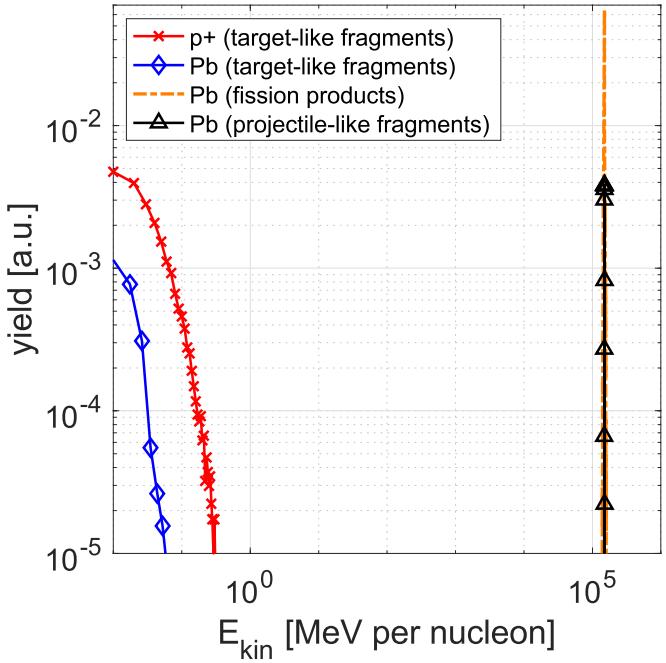

Fig. 9. Kinetic energy distribution of 150-GeV/n ^{208}Pb and 200-MeV protons on a 140-μm silicon target, focusing on target-like fragment, fission fragment, and primary particle contribution.

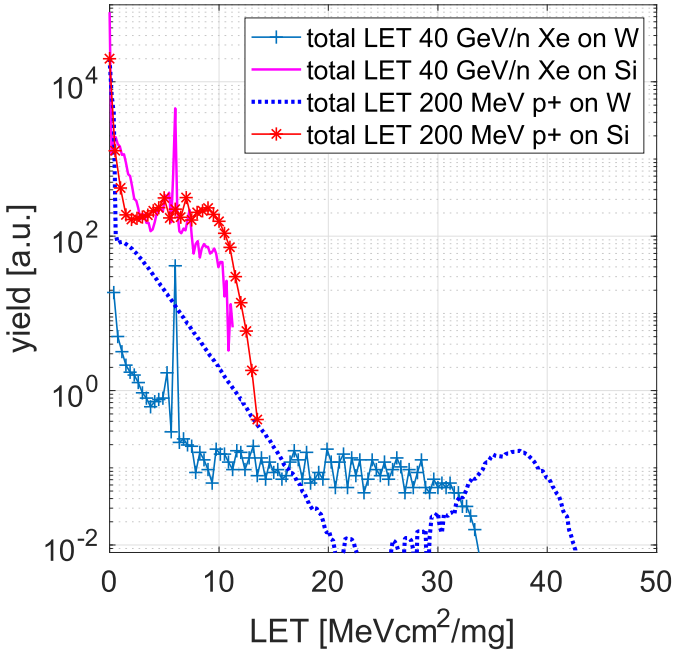

Fig. 10. LET distribution in silicon of 40-GeV/n ^{130}Xe and 200-MeV protons on a 140-μm silicon target and a 140-μm tungsten target.

very high LET, as previously discussed in Section II-C. This is caused by their increased mass after the fusion process.

A comparable phenomenon of fusion has been observed earlier for silicon on carbon [27]. In general, ions lose energy while traversing through matter mainly through ionization. However, if the incident particle energy is below the Coulomb barrier (which is tens of MeV above the corresponding Bragg peak energy and maximum LET of the incident particle in the material), the primary particle nucleus cannot interact with the target nucleus, due to the Coulomb repulsive force between them. Above this barrier, the nuclear collisions are more probable, like in the mentioned study, where 115-MeV ^{28}Si ions have been impinged on carbon. Fusion between silicon and carbon nucleii occurred, resulting in a compound nucleus. This phenomenon could only take place because the incident particle energy was twice the Coulomb barrier [25].

The argon Bragg peak in silicon is reached at 1.13 MeV/n, with a maximum LET of 18.65 MeVcm^2/mg [28]. According to the observations in [25], tens of MeV above this energy are needed to overcome the Coulomb barrier and to enable nucleus-nucleus reactions. Since the fusion products for argon have a kinetic energy of 5.0 MeV/n and are heavier than the primary particle or the target, the incident particle must have had an energy high enough to cause the fusion process and form a new compound Ar-Si-nucleus. For the case of neon, the energy reached by the fusion products is 1.9 MeV/n, more than twice the energy corresponding to the maximum LET of 8.95 MeVcm^2/mg [26], which is 0.8 MeV/n. Therefore, a compound nucleus is also created.

Concerning the interaction of protons and UHE HIs, the kinetic energy distribution of 150-GeV/n lead for nuclear fragments originated from target-like fragments ($12.5 < Z < 14.5$) and fission processes ($16.5 < Z < 80.5$) are illustrated in Fig. 9, together with the total and projectile fragments ($80.5 < Z < 84.5$). Target-like fragments originated from 200-MeV protons are also included in the same figure for comparison. Particles produced in the frame of the fission populate the main peak occurring at 150-GeV/n kinetic energy. Therefore, the fission products coming from the interaction between the primary beam and the silicon target have a similar kinetic energy per nucleon to the original projectile. Furthermore, the kinetic energy of fragments, having Z close to silicon, is very low and their LET is therefore very high, as opposed to the projectiles and fission-fragments.

Fission and projectile-like fragments produced by HIs like lead or xenon have a very high kinetic energy, comparable to the primary beam one. Hence, the corresponding LET of these fragments, despite the fact of being very heavy, is low. On the contrary, the target-like fragments have a very low kinetic energy, resulting in larger LET values.

To sum up, projectile ($80.5 < Z < 84.5$) and fission fragments ($16.5 < Z < 80.5$) produced by UHE HIs have a very large energy and therefore relatively low LET values. Contrarily, the target-like fragments produced during interaction between projectile and target material, show a low kinetic energy and high LET. In the case of protons, all fragments of interest for nuclear SEE induction are target-like.

E. Impact of Target Material on the Z and LET Distributions for High Energy Proton and UHE HI Beams

To investigate more the role of the target material with regard to its Z, the LET distribution in silicon of a 40-GeV/n xenon beam is shown in Fig. 10 while utilizing a 140-μm silicon target compared to a 140-μm tungsten target. Whereas the LET goes up to 12.5 MeVcm^2/mg in the case of the silicon target, it reaches a value close to 35 MeVcm^2/mg for a

tungsten target. Furthermore, the same peak can be observed at 6 MeVcm^2/mg for both target materials, associated with the primary beam.

For 200-MeV protons, the general behavior is similar to xenon in terms of difference between a silicon and tungsten target. However, even though the LET distribution of protons-on-silicon-fragments is easily comparable to xenon on silicon, in the case of tungsten as target material, the total proton LET reaches a value of 43 MeVcm^2/mg, which is even higher than the total LET of 40.5 MeVcm^2/mg in silicon achieved for 150-GeV/n lead on tungsten (note that this latter case is not included in the plot in order not to compromise its readability).

The main conclusion from Fig. 10 is that at high energies, HIs and protons produce a similar LET in silicon, for both a silicon and tungsten target. In other words, provided the high-LET fragments are of target-like type, they have a very weak dependence on the projectile, but strongly depend on the target material.

F. Z, LET, and Kinetic Energy Distributions for Other High Energy Ions Abundant in the GCR Environment

To complete the study related to high and UHE HIs, carbon and iron have been investigated, as well. Being very abundant in space, these two ion species play an important role for space application testing. Therefore, ^{12}C and ^{56}Fe of 1 GeV/n have been simulated focusing on the fragmentation mechanisms, as well as on the Z, LET, and kinetic energy distribution of the fragments. The energy has been chosen to mimic the most realistic conditions, because the flux spectra in the GCR environment reach its maximum flux around 1 GeV/n [3].

The Z distribution of ^{12}C extends up to $Z = 15$ and shows a peak at $Z = 6$, in correspondence with the atomic number of the target material ($Z_{Si} = 14$) and the projectile ($Z_C = 6$), respectively. Accordingly, the Z distribution for ^{56}Fe on silicon goes up to $Z = 27$ ($Z_{Fe} = 27$), whereas a peak is visible around $Z = 14$, which can be attributed again to the silicon contribution.

Looking at the LET distributions generated by these ions and their fragments, ^{12}C leads to a LET of 12 MeVcm^2/mg in total, mainly caused by the projectile itself. For ^{56}Fe, the LET goes up to 12 MeVcm^2/mg too, but in this case, the main contribution is due to fragments with $Z < 12$. Therefore, their overall behavior can be considered as analogous to the higher-Z UHE ions (Xe and Pb) studied in this article.

III. Sub-LET Threshold Ion SEE Modeling and Experimental Data

The impact of the nuclear interaction products on the SEE production is addressed in this work through the analysis of the SEL induced on a specific static random-access memory (SRAM) irradiated under the different beam conditions described in Sections I and II. Showing a high LET-threshold, the experimental study of a wide LET region could be performed. Moreover, the associated energy deposition mechanisms were investigated with the help of MC simulations. These simulations, dedicated to study the full transport, aimed at scoring the deposited energy in the SV [2] and convolving it with an SEL response function based on the direct ionization

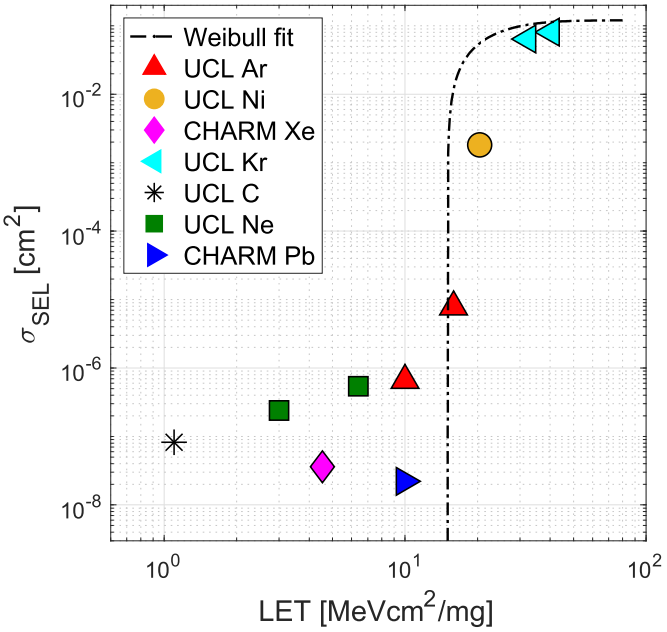

Fig. 11. FLUKA simulated sub-LET for HIs SEL cross section as a function of ion LET for a SRAM memory up to 150 GeV/n compared to experimental data.

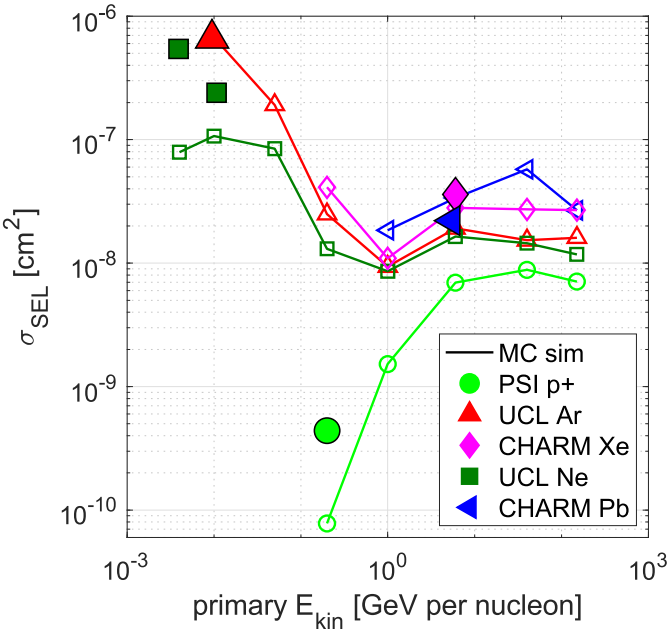

Fig. 12. FLUKA simulated sub-LET for HIs and proton SEL cross section as a function of ion energy for a SRAM memory up to 150 GeV/n compared to experimental data.

HI data. The resulting SEL cross section compared to experimental data from several test campaigns [3], [7], [29] of the selected high-LET SEL threshold memory can be seen in Figs. 11 and 12. Looking at these figures, it is relevant to note that the flux of HIs of the GCR spectra peaks at approximately 1 GeV/n. Therefore, for energies higher than that, the HIs are less abundant and therefore are causing fewer effects.

Fig. 11 shows the cross section as a function of LET for different simulated and measured ion data. In this illustration, the sub-LET region (LET below ~15 MeVcm^2/mg) can be found within the red box. The ion data outside have a LET above the sub-LET threshold, but has been included to give a full overview. Ions with similar LET values, but below

15 MeVcm^2/mg, are varying in their cross sections. Whereas for higher LET values, the cross sections show a stable behavior.

As opposed to Fig. 11, Fig. 12 is focused only on the sub-LET region showing the behavior of protons and various HI projectiles. For standard energy HI beams, such as neon and argon, inverse proportionality between the SEL cross section and the applied kinetic energy of the primary particle is observed for energies below 1 GeV/n. This can be attributed to the relevance in this energy range of the fragments generated by fusion, which has a decreasing probability with energy. For energies higher than 1 GeV/n, the distributions are comparable, and the saturation value is very similar for all the particle species, including high energy protons.

The HI SEL cross section decreases by almost two orders of magnitude between low and high energies. This can be explained again by the decreasing fusion interaction cross section. Above roughly 100 MeV/n and up to the maximum energies studied here, the sub-LET threshold SEL cross section is dominated by target fragments and is therefore constant and with similar absolute values for a very broad range of projectile Z-values [25], [30]. For the experimental data obtained in the 40-GeV/n Xe and 150-GeV/n Pb HI beams at CERN [8], [24], no SEL events were able to be observed for this component, due to the lower flux delivered in the SPS-NA, compared to CHARM [7].

As a next step, the influence of high-Z material has been investigated for several ions and energies. Previous studies [29] have shown that the presence of abundant tungsten in memories influences the observed SEL cross section (in particular in the sub-LET threshold region. In this study, the amount and location of the tungsten plugs was selected according to the scanning electron microscopy (SEM) analysis of the component. As an example, Fig. 13 shows the SEL cross section as a function of the kinetic energy of neon ions in GeV per nucleon, in the cases of the described model including tungsten (dashed blue) and when a silicon-only case is simulated (red).

The SEL cross section when silicon and tungsten are considered as target materials is higher than for the full-silicon target case, due to the higher atomic number Z of tungsten and the resulting higher LET fragments, as was shown in Fig. 10. It can be observed that for lower primary kinetic energies, the difference is smaller compared to higher energies. Moreover, the decrease in the cross section is more evident in the silicon curve, whereas for silicon and tungsten the cross section shows more steadiness over the whole range of energies. This can be explained by the behavior of the energy deposition distribution in silicon. For the case with silicon as target material, the maximum volume equivalent LET reaches a value of ~34 MeVcm^2/mg for an energy of 4 MeV/n, which is compatible with the neon-silicon fusion products, and decreases with energy, due to the reduction in fusion cross section.

Looking at the study of a standard memory tested for SEL design in Fig. 13, including silicon and tungsten, the fusion with tungsten already has a small impact on 4 MeV/n. However, the real influence is visible for 10 MeV/n, where the energy deposition reaches extremely large values. As for the only silicon case, this seems to be caused again by fusion between the neon ions and the target material. Additionally to the influence of fusion, fission might also play a role in these interactions, because for 50 MeV/n, the energy deposition might be originated from fission fragments, instead of fusion ones.

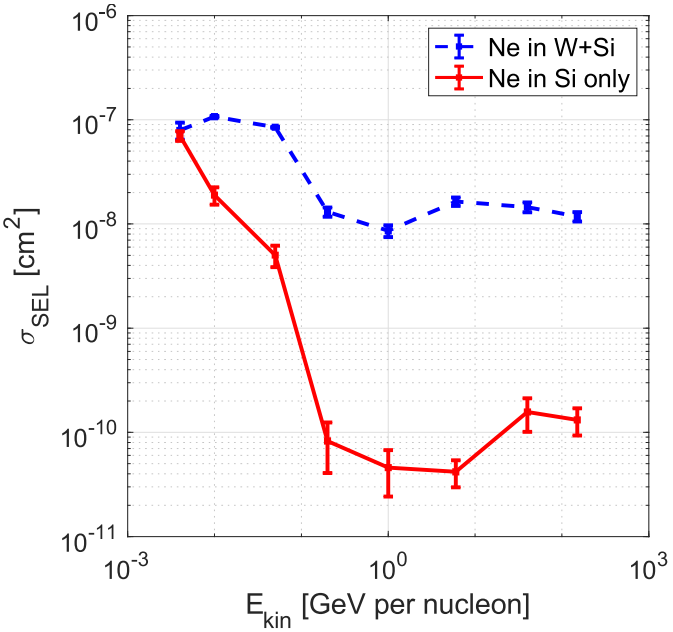

Fig. 13. FLUKA simulated sub-LET of ^{20}Ne for a SRAM memory (dashed blue) up to 150 GeV/n compared to a simulation after removing all tungsten (red).

IV. Discussion and Radiation Hardness Assurance Implications

The described physical processes on a nuclear interaction level for the broad particle and energy range presented in this article have significant implications for radiation hardness assurance. For standard energy HIs and high energy protons, which are widely used for space application SEE tests, the results presented in this article have shown that fusion products, with LET higher than the projectile, dominate as far as the sub-threshold LET region is concerned. This leads to a relatively high SEL cross section, as observed in this article, and as well as to a high SEE cross section in general. Therefore, the impact and influence of nuclear fragmentation products on SEE testing procedures should not be neglected.

Indeed, as shown in Figs. 3 and 4 and the related discussions, relatively low LET particles (e.g., 9.3-MeV/n neon, with an LET in silicon of 3.6 MeVcm^2/mg) can generate secondary ions with LETs of up to 22 MeVcm^2/mg. Therefore, it is likely that, for components whose SEE cross section is relatively low in this LET range (~10^{-6}cm^2/device), the experimentally observed events are in fact due to indirect ionization. However, as it is in principle not possible to directly distinguish between direct and indirect ionization in HI testing, such experimental points would be included in the standard SEE versus LET curve, thus having a strong impact on the derived LET threshold value and therefore also on the derived SEE rate. In other words, provided low-energy fusion effects are expected to be negligible in space, given

the overall dominance of higher energy ions, such low-LET experimental points, originated from low-energy ion fusion, would lead to a potentially significantly lower LET threshold value and overestimated predicted in-flight SEE rate.

Moreover, experimental results from the recent UHE HI test campaigns in the CERN accelerator complex in combination with MC simulation studies have confirmed that high-energy sub-LET threshold SEE events in space are expected to be strongly dominated by protons. Given that high-energy SEE cross sections of protons and HIs are similar, the significantly larger abundance of protons results in their dominance.

V. Conclusion and Outlook

This article, dedicated to sub-LET threshold nuclear interaction and fragmentation phenomena, has pointed out that the influence of created fragments should not be neglected when it comes to SEE tests. The impact of fusion products is significant, especially for standard energy HI beams, which are common for SEE space component tests. Related to this, it is relevant to underline the importance of MC tools and associated SEE models enabling the simulation of a broad variety of particle species and energies, as shown in Fig. 11. Since the GCR environment offers a broad variety of particle species and energies, accessing all experimentally for qualification purposes is unpractical. Therefore, it is important to combine standard test data and models. This would ensure being able to retrieve a realistic description of the SEE cross sections in the full ion energy and species phase space and to derive the associated SEE rate estimation implications.

Two main conclusions can be extracted from the study carried out in this article.

1) Standard energy (∼10 MeV/n) HIs will produce high-LET nuclear fragments, through fusion processes with target materials, and which are expected to dominate the sub-LET threshold SEE cross sections.
2) Very-high (100 MeV/n–5 GeV/n) and ultrahigh (5–150 GeV/n) energy ions will produce projectile-like and fission fragments with energies per nucleon similar to those of the projectile beam, and, therefore, with LET values similar or lower to it. Thus, the high-LET fragments of relevance to the sub-LET threshold SEE cross section correspond to low-energy target-like fragments, and, therefore, hardly depend on the Z of the incident ion.

Acknowledgment

The authors would like to thank the FLUKA Developer Team at CERN for support in this effort, especially Giulia Aricò.

References

[1] P. E. Dodd *et al.*, "Impact of heavy ion energy and nuclear interactions on single-event upset and latchup in integrated circuits," *IEEE Trans. Nucl. Sci.*, vol. 54, no. 6, pp. 2303–2311, Dec. 2007.
[2] R. A. Reed *et al.*, "Physical processes and applications of the Monte Carlo radiative energy deposition (MRED) code," *IEEE Trans. Nucl. Sci.*, vol. 62, no. 4, pp. 1441–1461, Aug. 2015.
[3] R. Garcia Alia *et al.*, "Proton dominance of sub-LET threshold GCR SEE rate," *IEEE Trans. Nucl. Sci.*, vol. 64, no. 1, pp. 388–397, Jan. 2017.
[4] E. Petersen, *Single Event Effects in Aerospace*. Hoboken, NJ, USA: Wiley, 2011.
[5] J. A. Pellish *et al.*, "Heavy ion testing with iron at 1 GeV/amu," *IEEE Trans. Nucl. Sci.*, vol. 57, no. 5, pp. 2948–2954, Oct. 2010.
[6] A. Ferrari, P. R. Sala, A. Fasso, and J. Ranft, *FLUKA: A Multi-Particle Transport Code (Program Version 2005)*. Geneva, Switzerland: CERN, 2005.
[7] P. Fernandez-Martinez *et al.*, "SEE tests with ultra energetic Xe ion beam in the CHARM facility at CERN," *IEEE Trans. Nucl. Sci.*, vol. 66, no. 7, pp. 1523–1531, Jul. 2019.
[8] R. G. Alia *et al.*, "Ultraenergetic heavy-ion beams in the CERN accelerator complex for radiation effects testing," *IEEE Trans. Nucl. Sci.*, vol. 66, no. 1, pp. 458–465, Jan. 2019.
[9] *Texas A&M University Cyclotron Institute Radiation Effects Facility*. Accessed: Dec. 11, 2019. [Online]. Available: https://cyclotron.tamu.edu/ref/
[10] *Berkeley Accelerator Space Effects—Lawrence Berkeley National Laboratory*. Accessed: Dec. 11, 2019. [Online]. Available:http://cyclotron.lbl.gov/base-rad-effects
[11] M.-H. Moscatello, A. Dubois, and X. Ledoux, "Industrial applications with GANIL SPIRAL2 facility," in *Proc. 16th Eur. Conf. Radiat. Effects Compon. Syst. (RADECS)*, Sep. 2016, pp. 1–3.
[12] *KVI—Center for Advanced Radiation Technology*. Accessed: Dec. 11, 2019. [Online]. Available: http://www.rug.nl/kvi-cart
[13] *GSI Helmholtzzentrum für Schwerionenforschung GmbH*. Accessed: Jan. 28, 2020. [Online]. Available: https://www.gsi.de/en/researchaccelerators.htm
[14] *NASA Space Radiation Laboratory at Brookhaven*. Accessed: Jan. 28, 2020. [Online]. Available: https://www.bnl.gov/nsrl/
[15] M. Stocker *et al.*, "Status of the PSI/ETH compact AMS facility," *Nucl. Instrum. Methods Phys. Res. B, Beam Interact. Mater. Atoms*, vols. 223–224, pp. 104–108, Aug. 2004.
[16] A. Virtanen, R. Harboe-Sorensen, A. Javanainen, H. Kettunen, H. Koivisto, and I. Riihimaki, "Upgrades for the RADEF facility," in *Proc. IEEE Radiat. Effects Data Workshop*, Jul. 2007, pp. 38–41.
[17] *Centre du Recherches du Cyclotron Universit Catholique de Louvain-la-Neuve*. Accessed: May 9, 2019. [Online]. Available: https://uclouvain.be/en/
[18] R. Koga, N. Katz, S. D. Pinkerton, W. A. Kolasinski, and D. L. Oberg, "Bevalac ion beam characterizations for single event phenomena," *IEEE Trans. Nucl. Sci.*, vol. 37, no. 6, pp. 1923–1928, Dec. 1990.
[19] G. Battistoni *et al.*, "Overview of the FLUKA code," *Ann. Nucl. Energy*, vol. 82, pp. 10–18, Aug. 2015.
[20] T. T. Böhlen *et al.*, "The FLUKA code: Developments and challenges for high energy and medical applications," *Nucl. Data Sheets*, vol. 120, pp. 211–214, Jun. 2014.
[21] S. Roesler, R. Engel, and J. Ranft, "The Monte Carlo event generator DPMJET-III," in *Advanced Monte Carlo for Radiation Physics, Particle Transport Simulation, and Applications*, A. Kling, F. J. C. Barao, M. Nakagawa, L. Tavora, and P. Vaz, Eds. Berlin, Germany: Springer, 2001, pp. 1033–1038.
[22] H. Sorge, H. Stöcker, and W. Greiner, "Poincaré invariant Hamiltonian dynamics: Modelling multi-hadronic interactions in a phase space approach," *Ann. Phys.*, vol. 192, no. 2, pp. 266–306, 1989.
[23] F. Cerutti *et al.*, "Low energy nucleus-nucleus reactions: The BME approach and its interface with FLUKA," in *Proc. Int. Conf. Nuclear Reaction Mech.*, Varenna, Italy, vol. 126, Jun. 2006, pp. 1–8.
[24] *European Component Irradiation Facilities Cocktail Calculator*. Accessed: Dec. 5, 2019. [Online]. Available: http://research.jyu.fi/radef/ECIFcalc/dedx.html
[25] C. Cazzaniga, R. G. Alía, M. Kastriotou, M. Cecchetto, P. Fernandez-Martinez, and C. D. Frost, "Study of the deposited energy spectra in silicon by high-energy neutron and mixed fields," *IEEE Trans. Nucl. Sci.*, submitted for publication.
[26] R. Koga, S. H. Crain, W. R. Crain, K. B. Crawford, and S. J. Hansel, "Comparative SEU sensitivities to relativistic heavy ions," *IEEE Trans. Nucl. Sci.*, vol. 45, no. 6, pp. 2475–2482, Dec. 1998.
[27] W. Von Oertzen, "Transfer of nucleons between heavy nuclei at large distances," presented at the Workshop Interface Between Nucl. Struct. Heavy-Ion Reaction Dyn., Notre Dame, IN, USA, May 1990. [Online]. Available: https://inis.iaea.org/search/search.aspx?orig_q=RN:23009817
[28] J. Ziegler. *SRIM & TRIM*. Accessed: Aug. 19, 2019. [Online]. Available: http://www.srim.org/
[29] R. G. Alia *et al.*, "Energy dependence of tungsten-dominated SEL cross sections," *IEEE Trans. Nucl. Sci.*, vol. 61, no. 5, pp. 2718–2726, Sep. 2014.
[30] R. G. Alia *et al.*, "SEL cross section energy dependence impact on the high energy accelerator failure rate," *IEEE Trans. Nucl. Sci.*, vol. 61, no. 6, pp. 2936–2944, Dec. 2014.